ELSEVIER

Applied Mathematical Modelling 27 (2003) 307–326

APPLIED MATHEMATICAL MODELLING

www.elsevier.com/locate/apm

Three-dimensional interfacial Green's functions in anisotropic bimaterials

E. Pan [*,1], B. Yang [2]

Structures Technology, Inc., 543 Keisler Dr., Suite 204, Cary, NC 27511, USA

Received 2 January 2002; accepted 1 November 2002

Abstract

In this paper, we derive, *for the first time*, the *complete* set of three-dimensional interfacial elastostatic Green's functions in anisotropic bimaterials, including displacements, stresses, and their derivatives with respect to the source coordinates. We make use of the extended Stroh formalism and the Mindlin's superposition method, and express these Green's functions in terms of one-dimensional finite-part integrals with variable θ over $[0,\pi]$. Denoting by r the distance between the field and source points on the interfacial planes, we show that the interfacial displacements, stresses and derivatives of displacements, and derivatives of stresses are proportional, respectively, to $1/r$, $1/r^2$, and $1/r^3$, while their finite-part integrals are, respectively, in the orders of $1/\cos\theta$, $1/\cos^2\theta$, and $1/\cos^3\theta$. Because of the special dependence upon the distance r, the interfacial Green's functions on the whole interfacial plane are completely determined by their values on the unit circle on the interfacial plane. An efficient and accurate method is also proposed for the evaluation of the involved finite-part integrals, and some typical numerical examples are given to show the general features of the interfacial Green's functions. In particular, it is remarked that some of them are discontinuous across the interface. These interfacial Green's functions are essential to various integral-equation methods in solving inclusion and interfacial crack problems in anisotropic bimaterials. Furthermore, they are also required in the study of strained quantum dot semiconductor devices should the Green's function method be applied.

Keywords: Interfacial Green's functions; 3D bimaterials; Finite-part integral; Stroh formalism; Anisotropic elasticity

* Corresponding author.

E-mail addresses: ernian_pan@yahoo.com, pan2@akron.edu (E. Pan).

[1] Present address: Department of Civil Engineering, The University of Akron, Akron, OH 44325-3905, USA.

[2] Present address: Materials Reliability Division, National Institute of Standards and Technology, Boulder, CO 80305, USA.

0307-904X/02/$ - see front matter
PII: S0307-904X(02)00126-9

1. Introduction

It is well known that Green's function is a key factor in various numerical methods based on the integral-equation formulation. When two materials are involved, the corresponding Green's function is called bimaterial Green's function. It is remarked that the bimaterial Green's function has certain distinct features as compared to the Green's functions in a homogeneous domain. In particular, depending upon the relative location of the source and field points, a total of four types of Green's functions are required in a bimaterial system [1,2], corresponding to the four different combinations of the domains of the source and field points. When both the source and field points are located on the interface of a bimaterial space, the corresponding Green's functions are specifically called interfacial Green's functions. However, even for this reduced case, all the four types of the Green's functions are still required (i.e., corresponding to the four interfacial planes). In other words, the relative location of the source and field points (i.e., the material domain) must be specifically defined even though some of the interfacial Green's functions are independent of the relative location of the source and field points. Interfacial Green's functions have particular applications in problems involving, for example, interlaminar stresses [3,4], surface responses in materials science [5,6] and earthquake/rock engineering [7–9], interfacial crack and contact [10–13], and inverse evaluation of materials properties using experimental approaches [6]. More recently, the Green's function method has been directly applied to the study of the strained quantum dot semiconductor devices [14]. Since a semiconductor device is commonly appeared as an anisotropic heterostructure (i.e., a layered structure) [15,16], the interfacial Green's function solution in anisotropic bimaterials is required should the Green's function method be employed.

In two-dimensional (2D) and generalized plane strain or plane stress deformations, interfacial Green's functions in generally anisotropic bimaterials can be deduced directly from the corresponding bimaterial Green's functions for which an exact closed-form solution exists [17]. Furthermore, Pan and Amadei [18] recently used the 2D interfacial Green's functions in their single-domain boundary integral-equation formulation for the analysis of 2D interfacial cracks.

In contrast to the 2D case, the corresponding 3D bimaterial Green's functions are much more complicated. To the best of the authors' knowledge, only for the case of isotropic material and of transversely isotropic material with symmetry plane parallel to the interface, have the 3D bimaterial Green's functions been developed in exact closed forms. Again, for these special cases, the interfacial Green's functions can be deduced directly from the bimaterial Green's functions by simply letting the source and field points approach the interface from either side of the interface.

For 3D generally anisotropic bimaterials, Ting [17] derived the interfacial displacements and tractions by applying the extended Stroh's formalism and 2D Fourier transforms. Since the source point is fixed on the interface $z = 0$, the resulting Green's functions in Ting [17] are independent of the third source coordinate (i.e., the coordinate in the z-direction). Consequently, the derivatives of these Green's displacements and tractions with respect to the source coordinate cannot be obtained.

More recently, Pan and Yuan [19] obtained the bimaterial Green's functions in 3D anisotropic bimaterials. By utilizing the Fourier inverse transform in the polar coordinate and combining with Mindlin's superposition method, they derived the physical-domain bimaterial Green's functions as a sum of a full-space Green's function in explicit form and a complementary part in terms of a

regular line integral over $[0,\pi]$. For the source point in material 1, the bimaterial and interfacial Green's displacements and stresses were derived by Pan and Yuan [19].

The purpose of this paper is to derive the *complete* set of the interfacial Green's functions in anisotropic bimaterials, including displacements, stresses, and their derivatives with respect to the source coordinates. For this goal, we first apply the inverse Fourier transforms to the bimaterial Green's functions in the Fourier transformed domain [17,19]. Derivatives of the resulting integrands are then taken with respect to the source coordinates. After taking the derivatives, both the source and field points are approached the interface (from their defined regions), and the corresponding interfacial solutions are derived. To handle the Fourier inverse transforms, the polar coordinate system is used [19]. In this system, integrals with respect to the infinite radial coordinate can be carried out analytically, by making use of some of the generalized integral expressions for the Dirac's delta function. In doing so, the final complete interfacial Green's functions in the physical domain can be expressed as 1D finite-part integrals over $[0,\pi]$.

Denoting by r the distance between the field and source points on the interfacial plane, we have showed that the present interfacial displacements, stresses and derivatives of displacements, and derivatives of stresses are proportional, respectively, to $1/r$, $1/r^2$, and $1/r^3$, with their finite-part integrals being, respectively, on the orders of $1/\cos\theta$, $1/\cos^2\theta$, and $1/\cos^3\theta$. Owing to the special dependence upon the distance r, the interfacial Green's functions in any one of the four entire interfacial planes (i.e., the combinations of $z=\pm 0$ and $d=\pm 0$ defined later) are completely determined by their values on the unit circle on the corresponding interfacial plane.

To evaluate the involved finite-part integral, an efficient and accurate numerical method is also proposed. Numerical examples are presented to illustrate the variation of some of the interfacial Green's functions along the unit circles on the interface planes (with the field point on the circle and source point at the center of the circle). These examples also clearly demonstrate the discontinuity features of some of the Green's functions across the interface.

2. Problem description and bimaterial Greens functions in Fourier transformed domain

Interfacial Green's function is a limit case of the corresponding bimaterial Green's function. Thus, to obtain the 3D interfacial Green's function, one can start with the corresponding bimaterial Green's function. However, taking the limit involves complicated mathematical operations, including integrals of generalized functions such as the Dirac's delta function. So far, no exact closed-from solution of such a 3D interfacial Green's function has been reported in the literature except for transversely isotropic and/or isotropic bimaterials.

We consider an anisotropic bimaterial full space where $x_3>0$ and $x_3<0$ are occupied by generally distinct materials 1 and 2, respectively. The interface is coincident with the plane $x_3=0$. The bimaterial system is loaded by a concentrated force $\boldsymbol{f}=(f_1,f_2,f_3)^{\mathrm{T}}$ at $\boldsymbol{d}=(d_1,d_2,d_3\equiv d)$ (the source point) in either one of the materials (Fig. 1), with the superscript T denoting the transpose. When the concentrated force $\boldsymbol{f}$ is applied, the equations of equilibrium are

$$\begin{aligned}&\sigma_{ij,j}=-f_i\delta(\boldsymbol{x}-\boldsymbol{d});\ \ \boldsymbol{x}\in\text{material 1}\\&\sigma_{ij,j}=0;\ \ \boldsymbol{x}\in\text{material 2}\end{aligned}\qquad(1a,b)$$

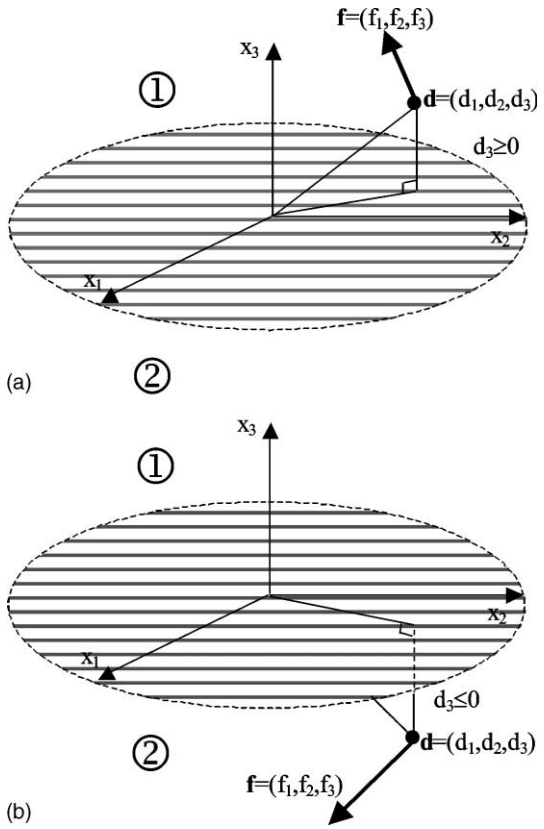

Fig. 1. A bimaterial system with source point in material 1 (a) and material 2 (b), respectively.

for the source point $\boldsymbol{d}$ in material 1, and

$$\begin{aligned} &\sigma_{ij,j} = 0; \ \boldsymbol{x} \in \text{material 1} \\ &\sigma_{ij,j} = -f_i \delta(\boldsymbol{x} - \boldsymbol{d}); \ \boldsymbol{x} \in \text{material 2} \end{aligned} \tag{2a, b}$$

for the source point $\boldsymbol{d}$ in material 2.

To derive the $\boldsymbol{f}$-induced bimaterial Green's function at a field point $\boldsymbol{x} = (x_1, x_2, x_3 \equiv z)$, the problem domain is divided artificially into three regions. For the source point in material 1, i.e., $d_3 > 0$, these three regions are: $x_3 > d_3$ (in material 1), $0 \leqslant x_3 < d_3$ (in material 1), and $x_3 < 0$ (in material 2). A similar division can be done for the source point in material 2, i.e., for $d_3 < 0$. We also note that the scalar variables z and d will be used exclusively for the third field coordinate x_3 and third source coordinate d_3, respectively.

The bimaterial Green's functions are therefore required to satisfy the equations of equilibrium (1) and (2), the continuity condition of displacement and traction across the interface ($z = 0$), continuity condition of displacement and jump condition of traction across the point source level ($z = d$), and the radiation condition as $|\boldsymbol{x}|$ approaches infinity [17,19]. To find the physical-domain bimaterial Green's functions, we first solve them in the Fourier transforms, as briefly presented below.

Defining the two-dimensional Fourier transforms for the horizontal field variables (x_1, x_2) as

$$\widetilde{u}_k(y_1, y_2, z) = \int_{-\infty}^{+\infty} \int_{-\infty}^{+\infty} u_k(x_1, x_2, z) \mathrm{e}^{\mathrm{i}y_\alpha x_\alpha} \, \mathrm{d}x_1 \, \mathrm{d}x_2 \tag{3}$$

where the repeated Greek subscript α takes the conventional summation from 1 to 2, and i, except for being used as an index, denotes the unit of imaginary number, $\sqrt{(-1)}$. In the following development, the polar coordinate expression for y_α, defined as

$$y_1 = \eta \cos\theta; \quad y_2 = \eta \sin\theta \tag{4}$$

will be also used.

Following Ting [17] and Pan and Yuan [19], the Fourier-domain general solutions of the displacement, traction (i.e., the out-of-plane stress on the $z =$ constant plane), and in-plane stress vectors in a homogeneous and anisotropic space can be derived as

$$\begin{aligned} \widetilde{\boldsymbol{u}}(y_1, y_2, z) &= \boldsymbol{a}\mathrm{e}^{-\mathrm{i}p\eta z} \\ \tilde{\boldsymbol{t}}(y_1, y_2, z) &= -\mathrm{i}\eta \boldsymbol{b}\mathrm{e}^{-\mathrm{i}p\eta z} \\ \tilde{\boldsymbol{s}}(y_1, y_2, z) &= -\mathrm{i}\eta \boldsymbol{c}\mathrm{e}^{-\mathrm{i}p\eta z} \end{aligned} \tag{5}$$

where the parameter p (also called eigenvalue), and vectors $\boldsymbol{a}$, $\boldsymbol{b}$ (also called eigenvectors), and $\boldsymbol{c}$ are functions of the anisotropic material properties of the solid and the polar angle θ defined in (4) [17,19], and $\tilde{\boldsymbol{t}}$ and $\tilde{\boldsymbol{s}}$ are the Fourier transforms of the traction and in-plane stress vectors defined by

$$\begin{aligned} \boldsymbol{t} &\equiv (\sigma_{13}, \sigma_{23}, \sigma_{33})^{\mathrm{T}} \\ \boldsymbol{s} &\equiv (\sigma_{11}, \sigma_{12}, \sigma_{22})^{\mathrm{T}} \end{aligned} \tag{6a, b}$$

The eigenvectors $\boldsymbol{a}_j$, and $\boldsymbol{b}_j$ are required to satisfy the following normalization relation [17,19].

$$\boldsymbol{b}_i^{\mathrm{T}}\boldsymbol{a}_j + \boldsymbol{a}_i^{\mathrm{T}}\boldsymbol{b}_j = \delta_{ij} \tag{7}$$

where the subscript j attached to the vectors $\boldsymbol{a}$ and $\boldsymbol{b}$ indicates the association of the eigenvectors to the corresponding eigenvalue p_j, and δ_{ij} is the Kronecker delta.

Expressing the general solutions in each of the three regions as a combination of solutions similar to (5), and making use of the continuity conditions at the interface, continuity/jump conditions at the source level, and the condition that the solutions should vanish as $|\boldsymbol{x}|$ approaches infinity, the bimaterial Green's functions in the transformed domain can then be derived [17, 19].

For source point in material 1 (i.e., $d > 0$), the three-region solutions are:

For $z > d$ (in material 1):

$$\begin{aligned} \widetilde{\boldsymbol{u}}_1(y_1, y_2, z; \boldsymbol{d}) &= -\mathrm{i}\eta^{-1}\overline{\boldsymbol{A}}_1\langle \mathrm{e}^{-\mathrm{i}\bar{p}_*^{(1)}\eta(z-d)}\rangle \bar{\boldsymbol{q}}_1^{\infty} - \mathrm{i}\eta^{-1}\overline{\boldsymbol{A}}_1\langle \mathrm{e}^{-\mathrm{i}\bar{p}_*^{(1)}\eta z}\rangle \bar{\boldsymbol{q}}_{11} \\ \tilde{\boldsymbol{t}}_1(y_1, y_2, z; \boldsymbol{d}) &= -\overline{\boldsymbol{B}}_1\langle \mathrm{e}^{-\mathrm{i}\bar{p}_*^{(1)}\eta(z-d)}\rangle \bar{\boldsymbol{q}}_1^{\infty} - \overline{\boldsymbol{B}}_1\langle \mathrm{e}^{-\mathrm{i}\bar{p}_*^{(1)}\eta z}\rangle \bar{\boldsymbol{q}}_{11} \\ \tilde{\boldsymbol{s}}_1(y_1, y_2, z; \boldsymbol{d}) &= -\overline{\boldsymbol{C}}_1\langle \mathrm{e}^{-\mathrm{i}\bar{p}_*^{(1)}\eta(z-d)}\rangle \bar{\boldsymbol{q}}_1^{\infty} - \overline{\boldsymbol{C}}_1\langle \mathrm{e}^{-\mathrm{i}\bar{p}_*^{(1)}\eta z}\rangle \bar{\boldsymbol{q}}_{11} \end{aligned} \tag{8}$$

For $0 \leqslant z < d$ (in material 1):

$$\begin{aligned}
\widetilde{\boldsymbol{u}}_1(y_1,y_2,z;\boldsymbol{d}) &= \mathrm{i}\eta^{-1}\boldsymbol{A}_1\langle \mathrm{e}^{-\mathrm{i}p_*^{(1)}\eta(z-d)}\rangle \boldsymbol{q}_1^{\infty} - \mathrm{i}\eta^{-1}\overline{\boldsymbol{A}}_1\langle \mathrm{e}^{-\mathrm{i}\bar{p}_*^{(1)}\eta z}\rangle \bar{\boldsymbol{q}}_{11} \\
\tilde{\boldsymbol{t}}_1(y_1,y_2,z;\boldsymbol{d}) &= \boldsymbol{B}_1\langle \mathrm{e}^{-\mathrm{i}p_*^{(1)}\eta(z-d)}\rangle \boldsymbol{q}_1^{\infty} - \overline{\boldsymbol{B}}_1\langle \mathrm{e}^{-\mathrm{i}\bar{p}_*^{(1)}\eta z}\rangle \bar{\boldsymbol{q}}_{11} \\
\tilde{\boldsymbol{s}}_1(y_1,y_2,z;\boldsymbol{d}) &= \boldsymbol{C}_1\langle \mathrm{e}^{-\mathrm{i}p_*^{(1)}\eta(z-d)}\rangle \boldsymbol{q}_1^{\infty} - \overline{\boldsymbol{C}}_1\langle \mathrm{e}^{-\mathrm{i}\bar{p}_*^{(1)}\eta z}\rangle \bar{\boldsymbol{q}}_{11}
\end{aligned} \tag{9}$$

For $z < 0$ (in material 2):

$$\begin{aligned}
\widetilde{\boldsymbol{u}}_2(y_1,y_2,z;\boldsymbol{d}) &= \mathrm{i}\eta^{-1}\boldsymbol{A}_2\langle \mathrm{e}^{-\mathrm{i}p_*^{(2)}\eta z}\rangle \boldsymbol{q}_{21} \\
\tilde{\boldsymbol{t}}_2(y_1,y_2,z;\boldsymbol{d}) &= \boldsymbol{B}_2\langle \mathrm{e}^{-\mathrm{i}p_*^{(2)}\eta z}\rangle \boldsymbol{q}_{21} \\
\tilde{\boldsymbol{s}}_2(y_1,y_2,z;\boldsymbol{d}) &= \boldsymbol{C}_2\langle \mathrm{e}^{-\mathrm{i}p_*^{(2)}\eta z}\rangle \boldsymbol{q}_{21}
\end{aligned} \tag{10}$$

Similarly, for the source point in material 2 (i.e., $d < 0$), the three-region solutions are:
For $z > 0$ (in material 1):

$$\begin{aligned}
\widetilde{\boldsymbol{u}}_1(y_1,y_2,z;\boldsymbol{d}) &= -\mathrm{i}\eta^{-1}\overline{\boldsymbol{A}}_1\langle \mathrm{e}^{-\mathrm{i}\bar{p}_*^{(1)}\eta z}\rangle \bar{\boldsymbol{q}}_{12} \\
\tilde{\boldsymbol{t}}_1(y_1,y_2,z;\boldsymbol{d}) &= -\overline{\boldsymbol{B}}_1\langle \mathrm{e}^{-\mathrm{i}\bar{p}_*^{(1)}\eta z}\rangle \bar{\boldsymbol{q}}_{12} \\
\tilde{\boldsymbol{s}}_1(y_1,y_2,z;\boldsymbol{d}) &= -\overline{\boldsymbol{C}}_1\langle \mathrm{e}^{-\mathrm{i}\bar{p}_*^{(1)}\eta z}\rangle \bar{\boldsymbol{q}}_{12}
\end{aligned} \tag{11}$$

For $d < z \leqslant 0$ (in material 2):

$$\begin{aligned}
\widetilde{\boldsymbol{u}}_2(y_1,y_2,z;\boldsymbol{d}) &= -\mathrm{i}\eta^{-1}\overline{\boldsymbol{A}}_2\langle \mathrm{e}^{-\mathrm{i}\bar{p}_*^{(2)}\eta(z-d)}\rangle \bar{\boldsymbol{q}}_2^{\infty} + \mathrm{i}\eta^{-1}\boldsymbol{A}_2\langle \mathrm{e}^{-\mathrm{i}p_*^{(2)}\eta z}\rangle \boldsymbol{q}_{22} \\
\tilde{\boldsymbol{t}}_2(y_1,y_2,z;\boldsymbol{d}) &= -\overline{\boldsymbol{B}}_2\langle \mathrm{e}^{-\mathrm{i}\bar{p}_*^{(2)}\eta(z-d)}\rangle \bar{\boldsymbol{q}}_2^{\infty} + \boldsymbol{B}_2\langle \mathrm{e}^{-\mathrm{i}p_*^{(2)}\eta z}\rangle \boldsymbol{q}_{22} \\
\tilde{\boldsymbol{s}}_2(y_1,y_2,z;\boldsymbol{d}) &= -\overline{\boldsymbol{C}}_2\langle \mathrm{e}^{-\mathrm{i}\bar{p}_*^{(2)}\eta(z-d)}\rangle \bar{\boldsymbol{q}}_2^{\infty} + \boldsymbol{C}_2\langle \mathrm{e}^{-\mathrm{i}p_*^{(2)}\eta z}\rangle \boldsymbol{q}_{22}
\end{aligned} \tag{12}$$

For $z < d$ (in material 2):

$$\begin{aligned}
\widetilde{\boldsymbol{u}}_2(y_1,y_2,z;\boldsymbol{d}) &= \mathrm{i}\eta^{-1}\boldsymbol{A}_2\langle \mathrm{e}^{-\mathrm{i}p_*^{(2)}\eta(z-d)}\rangle \boldsymbol{q}_2^{\infty} + \mathrm{i}\eta^{-1}\boldsymbol{A}_2\langle \mathrm{e}^{-\mathrm{i}p_*^{(2)}\eta z}\rangle \boldsymbol{q}_{22} \\
\tilde{\boldsymbol{t}}_2(y_1,y_2,z;\boldsymbol{d}) &= \boldsymbol{B}_2\langle \mathrm{e}^{-\mathrm{i}p_*^{(2)}\eta(z-d)}\rangle \boldsymbol{q}_2^{\infty} + \boldsymbol{B}_2\langle \mathrm{e}^{-\mathrm{i}p_*^{(2)}\eta z}\rangle \boldsymbol{q}_{22} \\
\tilde{\boldsymbol{s}}_2(y_1,y_2,z;\boldsymbol{d}) &= \boldsymbol{C}_2\langle \mathrm{e}^{-\mathrm{i}p_*^{(2)}\eta(z-d)}\rangle \boldsymbol{q}_2^{\infty} + \boldsymbol{C}_2\langle \mathrm{e}^{-\mathrm{i}p_*^{(2)}\eta z}\rangle \boldsymbol{q}_{22}
\end{aligned} \tag{13}$$

In (8)–(13), the dependence of the Green's functions upon the source point is indicated by the source point vector $\boldsymbol{d}$. Also in these expressions, the subscripts 1 and 2, and (1) and (2) denote the quantities in materials 1 and 2, respectively, and

$$\boldsymbol{q}_j^{\infty} = \boldsymbol{A}_j^{\mathrm{T}}\boldsymbol{f}\ \mathrm{e}^{\mathrm{i}y_\alpha d_\alpha}, \quad \bar{\boldsymbol{q}}_j^{\infty} = \overline{\boldsymbol{A}}_j^{\mathrm{T}}\boldsymbol{f}\ \mathrm{e}^{\mathrm{i}y_\alpha d_\alpha};\ \ j = 1,2 \tag{14a, b}$$

$$\langle \mathrm{e}^{-\mathrm{i}p_*\eta z}\rangle = \mathrm{diag}[\mathrm{e}^{-\mathrm{i}p_1\eta z}, \mathrm{e}^{-\mathrm{i}p_2\eta z}, \mathrm{e}^{-\mathrm{i}p_3\eta z}] \tag{15}$$

Furthermore, the complex vectors $\bar{\boldsymbol{q}}_{11}$ and $\boldsymbol{q}_{21}$ in (8)–(10) are given by

$$\begin{aligned}
\bar{\boldsymbol{q}}_{11} &= \boldsymbol{G}_1^{(1)}\langle \mathrm{e}^{\mathrm{i}p_*^{(1)}\eta d}\rangle \boldsymbol{A}_1^{\mathrm{T}}\boldsymbol{f}\ \mathrm{e}^{\mathrm{i}y_\alpha d_\alpha} \\
\boldsymbol{q}_{21} &= \boldsymbol{G}_2^{(1)}\langle \mathrm{e}^{\mathrm{i}p_*^{(1)}\eta d}\rangle \boldsymbol{A}_1^{\mathrm{T}}\boldsymbol{f}\ \mathrm{e}^{\mathrm{i}y_\alpha d_\alpha}
\end{aligned} \tag{16}$$

and $\bar{\boldsymbol{q}}_{12}$ and $\boldsymbol{q}_{22}$ in (11)–(13) by

$$\begin{aligned}\bar{\boldsymbol{q}}_{12} &= \boldsymbol{G}_1^{(2)}\langle \mathrm{e}^{\mathrm{i}\bar{p}_*^{(2)}\eta d}\rangle \overline{\boldsymbol{A}}_2^{\mathrm{T}}\boldsymbol{f}\ \mathrm{e}^{\mathrm{i}y_\alpha d_\alpha}\\ \boldsymbol{q}_{22} &= \boldsymbol{G}_2^{(2)}\langle \mathrm{e}^{\mathrm{i}\bar{p}_*^{(2)}\eta d}\rangle \overline{\boldsymbol{A}}_2^{\mathrm{T}}\boldsymbol{f}\ \mathrm{e}^{\mathrm{i}y_\alpha d_\alpha}\end{aligned} \tag{17}$$

In (16) and (17), the four $\boldsymbol{G}$ matrices are defined as

$$\begin{aligned}\boldsymbol{G}_1^{(1)} &= \overline{\boldsymbol{A}}_1^{-1}(\overline{\boldsymbol{M}}_1+\boldsymbol{M}_2)^{-1}(\boldsymbol{M}_2-\boldsymbol{M}_1)\boldsymbol{A}_1\\ \boldsymbol{G}_2^{(1)} &= \boldsymbol{A}_2^{-1}(\overline{\boldsymbol{M}}_1+\boldsymbol{M}_2)^{-1}(\boldsymbol{M}_1+\overline{\boldsymbol{M}}_1)\boldsymbol{A}_1\end{aligned} \tag{18}$$

$$\begin{aligned}\boldsymbol{G}_1^{(2)} &= \overline{\boldsymbol{A}}_1^{-1}(\overline{\boldsymbol{M}}_1+\boldsymbol{M}_2)^{-1}(\boldsymbol{M}_2+\overline{\boldsymbol{M}}_2)\overline{\boldsymbol{A}}_2\\ \boldsymbol{G}_2^{(2)} &= \boldsymbol{A}_2^{-1}(\overline{\boldsymbol{M}}_1+\boldsymbol{M}_2)^{-1}(\overline{\boldsymbol{M}}_1-\overline{\boldsymbol{M}}_2)\overline{\boldsymbol{A}}_2\end{aligned} \tag{19}$$

where $\boldsymbol{M}_\alpha$ is the impedance tensor defined as

$$\boldsymbol{M}_\alpha = -\mathrm{i}\boldsymbol{B}_\alpha\boldsymbol{A}_\alpha^{-1} \quad (\alpha=1,2) \tag{20}$$

with $\alpha=1$ and 2 denoting quantities in materials 1 and 2 respectively, and the matrices $\boldsymbol{A}$, $\boldsymbol{B}$, and $\boldsymbol{C}$ in (8)–(20) being defined as

$$\boldsymbol{A}=[\boldsymbol{a}_1,\boldsymbol{a}_2,\boldsymbol{a}_3],\quad \boldsymbol{B}=[\boldsymbol{b}_1,\boldsymbol{b}_2,\boldsymbol{b}_3],\quad \boldsymbol{C}=[\boldsymbol{c}_1,\boldsymbol{c}_2,\boldsymbol{c}_3] \tag{21}$$

In addition, in (8)–(13), (18) and (19), the superscript '−1' denotes the matrix inverse and the over bar the complex conjugate.

3. Interfacial Greens functions in physical domain

To derive the physical-domain interfacial Green's functions, we first apply the inverse Fourier transforms to the Fourier-domain solutions (8)–(13), and then take the derivatives of the solutions with respect to the source coordinates ($d_1, d_2, d_3 \equiv d$). After taking the derivatives, the source and field points can both approach the interface (from their defined regions). Similar to the procedure of deriving the bimaterial Green's functions, the polar coordinate transform defined by (4) can be introduced so that the infinite integral with respect to the radial variable can be carried out analytically. Consequently, the final interfacial Green's functions in the physical domain can be expressed in terms of 1D finite-part integrals over $[0,\pi]$.

As an illustration, we derive the physical-domain interfacial Green's displacement and its derivatives with respect to the source coordinates in region $z>d$ of material 1 due to a point force vector $\boldsymbol{f}$ in material 1. All other Green's functions can be derived similarly.

Applying the Fourier inverse transform, the bimaterial Green's displacement in the physical domain, for both the field point $\boldsymbol{x}=(x_1,x_2,z)$ and source point $\boldsymbol{d}=(d_1,d_2,d)$ in material 1, can be expressed as

$$\begin{aligned}\boldsymbol{u}_1(\boldsymbol{x};\boldsymbol{d}) = &-\frac{\mathrm{i}}{4\pi^2}\int_{-\infty}^{+\infty}\int_{-\infty}^{+\infty}\left\{\eta^{-1}\overline{\boldsymbol{A}}_1\langle \mathrm{e}^{-\mathrm{i}\bar{p}_*^{(1)}\eta(z-d)}\rangle\bar{\boldsymbol{q}}_1^{\infty}\mathrm{e}^{-\mathrm{i}(x_\alpha-d_\alpha)y_\alpha}\right\}\mathrm{d}y_1\,\mathrm{d}y_2\\ &-\frac{i}{4\pi^2}\int_{-\infty}^{+\infty}\int_{-\infty}^{+\infty}\left\{\eta^{-1}\overline{\boldsymbol{A}}_1\langle \mathrm{e}^{-\mathrm{i}\bar{p}_*^{(1)}\eta z}\rangle\bar{\boldsymbol{q}}_{11}\mathrm{e}^{-\mathrm{i}(x_\alpha-d_\alpha)y_\alpha}\right\}\mathrm{d}y_1\,\mathrm{d}y_2\end{aligned} \tag{22}$$

The first integral in this equation corresponds to the full-space Green's displacement that is available in an explicit form [20,21]. Consequently, the inverse transform needs to be carried out only for the second regular integral, or the complementary part. Denoting the full-space Green's function by $\boldsymbol{u}_1^{\infty}(x_1,x_2,z)$ and making use of the polar coordinate transform (4), (22) then becomes

$$\boldsymbol{u}_1(\boldsymbol{x};\boldsymbol{d}) = \boldsymbol{u}_1^{\infty}(\boldsymbol{x};\boldsymbol{d}) - \frac{\mathrm{i}}{2\pi^2}\left[\int_0^{\pi}\mathrm{d}\theta\int_0^{\infty}\overline{\boldsymbol{A}}_1\langle \mathrm{e}^{-\mathrm{i}\bar{p}_*^{(1)}\eta z}\rangle \boldsymbol{G}_1^{(1)}\langle \mathrm{e}^{\mathrm{i}p_*^{(1)}\eta d}\rangle \mathrm{e}^{-\mathrm{i}\eta[(x_1-d_1)\cos\theta+(x_2-d_2)\sin\theta]}\boldsymbol{A}_1^{\mathrm{T}}\,\mathrm{d}\eta\right]\boldsymbol{f} \tag{23}$$

where the periodicity of the involved integrands has been utilized to reduce the angular integral from $[0,2\pi]$ to $[0,\pi]$ [22].

Now, taking the derivative of the Green's displacement with respect to the source coordinates $(d_1,d_2,d_3\equiv d)$, we obtain [3]

$$\begin{aligned}\frac{\partial \boldsymbol{u}_1(\boldsymbol{x};\boldsymbol{d})}{\partial d_j} &= \frac{\partial \boldsymbol{u}_1^{\infty}(\boldsymbol{x};\boldsymbol{d})}{\partial d_j}\\ &\quad + \frac{1}{2\pi^2}\left[\int_0^{\pi}\mathrm{d}\theta\int_0^{\infty}\eta\overline{\boldsymbol{A}}_1\langle \mathrm{e}^{-\mathrm{i}\bar{p}_*^{(1)}\eta z}\rangle \boldsymbol{G}_1^{(1)}\left\langle g_j^{(1)}\right\rangle\langle \mathrm{e}^{\mathrm{i}p_*^{(1)}\eta d}\rangle \mathrm{e}^{-\mathrm{i}\eta[(x_1-d_1)\cos\theta+(x_2-d_2)\sin\theta]}\boldsymbol{A}_1^{\mathrm{T}}\,\mathrm{d}\eta\right]\boldsymbol{f}\end{aligned} \tag{24}$$

where

$$\begin{aligned}\left\langle g_1^{(1)}\right\rangle &= \mathrm{diag}[\cos\theta,\cos\theta,\cos\theta]\\ \left\langle g_2^{(1)}\right\rangle &= \mathrm{diag}[\sin\theta,\sin\theta,\sin\theta]\\ \left\langle g_3^{(1)}\right\rangle &= \mathrm{diag}[p_1^{(1)},p_2^{(1)},p_3^{(1)}]\end{aligned} \tag{25}$$

for the source point in material 1. For the source point in material 2, we have

$$\begin{aligned}\left\langle g_1^{(2)}\right\rangle &= \mathrm{diag}[\cos\theta,\cos\theta,\cos\theta]\\ \left\langle g_2^{(2)}\right\rangle &= \mathrm{diag}[\sin\theta,\sin\theta,\sin\theta]\\ \left\langle g_3^{(2)}\right\rangle &= \mathrm{diag}[\bar{p}_1^{(2)},\bar{p}_2^{(2)},\bar{p}_3^{(2)}]\end{aligned} \tag{26}$$

Let the field level z and source level d approach the interface from above, (23) and (24) then can be simplified as

$$\begin{aligned}\boldsymbol{u}_1(\boldsymbol{x};\boldsymbol{d})\Big|_{(z,d)=(0+,0+)} &= \boldsymbol{u}_1^{\infty}(\boldsymbol{x};\boldsymbol{d})\Big|_{(z,d)=(0+,0+)}\\ &\quad - \frac{\mathrm{i}}{2\pi^2}\left[\int_0^{\pi}\mathrm{d}\theta\int_0^{\infty}\overline{\boldsymbol{A}}_1\boldsymbol{G}_1^{(1)}\mathrm{e}^{-\mathrm{i}\eta[(x_1-d_1)\cos\theta+(x_2-d_2)\sin\theta]}\boldsymbol{A}_1^{\mathrm{T}}\,\mathrm{d}\eta\right]\boldsymbol{f}\end{aligned} \tag{27}$$

[3] Thereafter, the Latin index j takes range from 1 to 3, and the Greek index α from 1 to 2.

$$\frac{\partial \boldsymbol{u}_1(\boldsymbol{x};\boldsymbol{d})}{\partial d_j}\Big|_{(z,d)=(0+,0+)} = \frac{\partial \boldsymbol{u}_1^{\infty}(\boldsymbol{x};\boldsymbol{d})}{\partial d_j}\Big|_{(z,d)=(0+,0+)} + \frac{1}{2\pi^2}\left[\int_0^{\pi} \mathrm{d}\theta \int_0^{\infty} \overline{\boldsymbol{A}}_1 \boldsymbol{G}_1^{(1)} \left\langle g_j^{(1)} \right\rangle \boldsymbol{A}_1^{\mathrm{T}} \eta \mathrm{e}^{-\mathrm{i}\eta[(x_1-d_1)\cos\theta+(x_2-d_2)\sin\theta]}\,\mathrm{d}\eta\right]\boldsymbol{f} \tag{28}$$

Again, the first term on the right-hand side of (27) and (28) is the infinite Green's function that can be calculated very accurately and efficiently using an analytical approach without numerical integration [21]. Therefore, what we need to take care of is the integral of the second term on the right-hand side of (27) and (28). It is obvious that these integrals exist only in the sense of the generalized function. Furthermore, these integrals are very complicated to carry out and require integration by part for the Dirac's delta functions expressed as

$$\int_0^{\infty} \mathrm{e}^{-\mathrm{i}k\eta}\,\mathrm{d}\eta = -\frac{\mathrm{i}}{k} + \pi\delta(k) \tag{29}$$

$$\int_0^{\infty} \eta \mathrm{e}^{-\mathrm{i}k\eta}\,\mathrm{d}\eta = -\frac{1}{k^2} + \mathrm{i}\pi\frac{\mathrm{d}\delta(k)}{\mathrm{d}k} \tag{30}$$

$$\int_0^{\infty} \eta^2 \mathrm{e}^{-\mathrm{i}k\eta}\,\mathrm{d}\eta = \frac{2\mathrm{i}}{k^3} - \pi\frac{\mathrm{d}^2\delta(k)}{\mathrm{d}k^2} \tag{31}$$

To simplify the final expression, another polar coordinate transform (for the horizontal field and source points), as defined below, is also used.

$$x_1 - d_1 = r\cos\theta_0; \quad x_2 - d_2 = r\sin\theta_0 \tag{32}$$

Therefore, by carrying out the integrals with respect to η (including integration by part), the interfacial Green's displacement and its derivative with respect to the source coordinates (with both the field and source points in material 1) can finally be derived, which are expressed in terms of 1D finite-part integrals over $[0,\pi]$. In the following, we only present the final expressions for all the interfacial Green's functions while in Appendix A the key steps involved in obtaining the derivative of the Green's tractions with respect to the source coordinates are briefly outlined. It is noticed from Appendix A that the procedure of obtaining the derivatives of the Green's tractions is very complicated. Using the corresponding capital letter for the Green's tensor (3×3 matrix) with the row or the first index for the component of the physical quantity and the column or the second index for the point force direction, we then have

$$\boldsymbol{U}\left(\boldsymbol{x}^{(1)};\boldsymbol{d}^{(1)}\right) = \boldsymbol{U}^{\infty}\left(\boldsymbol{x}^{(1)};\boldsymbol{d}^{(1)}\right) - \frac{1}{2\pi r}\left\{\frac{1}{\pi}\int_0^{\pi} \frac{\overline{\boldsymbol{A}}_1 \boldsymbol{G}_1^{(1)} \boldsymbol{A}_1^{\mathrm{T}}}{\cos(\theta-\theta_0)}\,\mathrm{d}\theta + \mathrm{i}\left[\overline{\boldsymbol{A}}_1 \boldsymbol{G}_1^{(1)} \boldsymbol{A}_1^{\mathrm{T}}\right]_{\theta=\theta_0+\pi/2}\right\} \tag{33}$$

$$\frac{\partial \boldsymbol{U}\left(\boldsymbol{x}^{(1)};\boldsymbol{d}^{(1)}\right)}{\partial d_j} = \frac{\partial \boldsymbol{U}^{\infty}\left(\boldsymbol{x}^{(1)};\boldsymbol{d}^{(1)}\right)}{\partial d_j} - \frac{1}{2\pi r^2}\left\{\frac{1}{\pi}\int_0^{\pi} \frac{\overline{\boldsymbol{A}}_1 \boldsymbol{G}_1^{(1)} \left\langle g_j^{(1)} \right\rangle \boldsymbol{A}_1^{\mathrm{T}}}{\cos^2(\theta-\theta_0)}\,\mathrm{d}\theta - \mathrm{i}\frac{\mathrm{d}\left[\overline{\boldsymbol{A}}_1 \boldsymbol{G}_1^{(1)} \left\langle g_j^{(1)} \right\rangle \boldsymbol{A}_1^{\mathrm{T}}\right]}{\mathrm{d}\theta}\Big|_{\theta=\theta_0+\pi/2}\right\} \tag{34}$$

where $(\boldsymbol{x}^{(1)};\boldsymbol{d}^{(1)})$ indicates that the two-point interfacial Green's functions are for the field point $\boldsymbol{x}$ in material 1 and source point $\boldsymbol{d}$ in material 1. While the integral in (33) is Cauchy-type singular, that in (34) is hypersingular. Numerical treatment of these integrals requires special attention [23–25], which will be discussed in the next section. We mention that Pan and Yuan [19] derived a similar expression for the interfacial Green's displacement (33), which is an extension of the surface Green's displacement on the surface of an anisotropic half-space derived previously by Barnett and Lothe [5], Ting [17], and Wu [26].

Following the same procedure, the corresponding stress and stress derivatives are found to be

$$\boldsymbol{T}\left(\boldsymbol{x}^{(1)};\boldsymbol{d}^{(1)}\right)=\boldsymbol{T}^{\infty}\left(\boldsymbol{x}^{(1)};\boldsymbol{d}^{(1)}\right)+\frac{1}{2\pi r^2}\left\{\frac{1}{\pi}\int_0^{\pi}\frac{\overline{\boldsymbol{B}}_1\boldsymbol{G}_1^{(1)}\boldsymbol{A}_1^{\mathrm{T}}}{\cos^2(\theta-\theta_0)}\,\mathrm{d}\theta-\mathrm{i}\frac{\mathrm{d}\left[\overline{\boldsymbol{B}}_1\boldsymbol{G}_1^{(1)}\boldsymbol{A}_1^{\mathrm{T}}\right]}{\mathrm{d}\theta}\bigg|_{\theta=\theta_0+\pi/2}\right\} \tag{35}$$

$$\frac{\partial\boldsymbol{T}\left(\boldsymbol{x}^{(1)};\boldsymbol{d}^{(1)}\right)}{\partial d_j}=\frac{\partial\boldsymbol{T}^{\infty}\left(\boldsymbol{x}^{(1)};\boldsymbol{d}^{(1)}\right)}{\partial d_j}+\frac{1}{2\pi r^3}\left\{\frac{2}{\pi}\int_0^{\pi}\frac{\overline{\boldsymbol{B}}_1\boldsymbol{G}_1^{(1)}\left\langle g_j^{(1)}\right\rangle\boldsymbol{A}_1^{\mathrm{T}}}{\cos^3(\theta-\theta_0)}\mathrm{d}\theta+\mathrm{i}\left[\frac{\mathrm{d}^2\left[\overline{\boldsymbol{B}}_1\boldsymbol{G}_1^{(1)}\left\langle g_j^{(1)}\right\rangle\boldsymbol{A}_1^{\mathrm{T}}\right]}{\mathrm{d}^2\theta}+\left[\overline{\boldsymbol{B}}_1\boldsymbol{G}_1^{(1)}\left\langle g_j^{(1)}\right\rangle\boldsymbol{A}_1^{\mathrm{T}}\right]\right]\bigg|_{\theta=\theta_0+\pi/2}\right\} \tag{36}$$

$$\boldsymbol{S}\left(\boldsymbol{x}^{(1)};\boldsymbol{d}^{(1)}\right)=\boldsymbol{S}^{\infty}\left(\boldsymbol{x}^{(1)};\boldsymbol{d}^{(1)}\right)+\frac{1}{2\pi r^2}\left\{\frac{1}{\pi}\int_0^{\pi}\frac{\overline{\boldsymbol{C}}_1\boldsymbol{G}_1^{(1)}\boldsymbol{A}_1^{\mathrm{T}}}{\cos^2(\theta-\theta_0)}\,\mathrm{d}\theta-\mathrm{i}\frac{\mathrm{d}\left[\overline{\boldsymbol{C}}_1\boldsymbol{G}_1^{(1)}\boldsymbol{A}_1^{\mathrm{T}}\right]}{\mathrm{d}\theta}\bigg|_{\theta=\theta_0+\pi/2}\right\} \tag{37}$$

$$\frac{\partial\boldsymbol{S}\left(\boldsymbol{x}^{(1)};\boldsymbol{d}^{(1)}\right)}{\partial d_j}=\frac{\partial\boldsymbol{S}^{\infty}\left(\boldsymbol{x}^{(1)};\boldsymbol{d}^{(1)}\right)}{\partial d_j}+\frac{1}{2\pi r^3}\left\{\frac{2}{\pi}\int_0^{\pi}\frac{\overline{\boldsymbol{C}}_1\boldsymbol{G}_1^{(1)}\left\langle g_j^{(1)}\right\rangle\boldsymbol{A}_1^{\mathrm{T}}}{\cos^3(\theta-\theta_0)}\,\mathrm{d}\theta+\mathrm{i}\left[\frac{\mathrm{d}^2\left[\overline{\boldsymbol{C}}_1\boldsymbol{G}_1^{(1)}\left\langle g_j^{(1)}\right\rangle\boldsymbol{A}_1^{\mathrm{T}}\right]}{\mathrm{d}^2\theta}+\left[\overline{\boldsymbol{C}}_1\boldsymbol{G}_1^{(1)}\left\langle g_j^{(1)}\right\rangle\boldsymbol{A}_1^{\mathrm{T}}\right]\right]\bigg|_{\theta=\theta_0+\pi/2}\right\} \tag{38}$$

It is observed that the derivative of stresses ((36) and (38)) involves a third-order singularity. Although this high-order singularity was previously discussed mathematically, yet its direct connection to a physical quantity has never been appeared in the literature. Here we have shown, for the first time, that a third-order singular integral can be physically connected to the derivative of the interfacial stress.

Similarly, for the field point in material 2 and source point in material 1, we obtain [4]:

$$\begin{aligned}
&\boldsymbol{U}\left(\boldsymbol{x}^{(2)};\boldsymbol{d}^{(1)}\right)=\boldsymbol{U}\left(\boldsymbol{x}^{(1)};\boldsymbol{d}^{(1)}\right); \quad \frac{\partial \boldsymbol{U}\left(\boldsymbol{x}^{(2)};\boldsymbol{d}^{(1)}\right)}{\partial d_j}=\frac{\partial \boldsymbol{U}\left(\boldsymbol{x}^{(1)};\boldsymbol{d}^{(1)}\right)}{\partial d_j}\\
&\boldsymbol{T}\left(\boldsymbol{x}^{(2)};\boldsymbol{d}^{(1)}\right)=\boldsymbol{T}\left(\boldsymbol{x}^{(1)};\boldsymbol{d}^{(1)}\right); \quad \frac{\partial \boldsymbol{T}\left(\boldsymbol{x}^{(2)};\boldsymbol{d}^{(1)}\right)}{\partial d_j}=\frac{\partial \boldsymbol{T}\left(\boldsymbol{x}^{(1)};\boldsymbol{d}^{(1)}\right)}{\partial d_j}
\end{aligned} \tag{39}$$

$$\boldsymbol{S}\left(\boldsymbol{x}^{(2)};\boldsymbol{d}^{(1)}\right)=-\frac{1}{2\pi r^2}\left\{\frac{1}{\pi}\int_0^{\pi}\frac{\boldsymbol{C}_2\boldsymbol{G}_2^{(1)}\boldsymbol{A}_1^{\mathrm{T}}}{\cos^2(\theta-\theta_0)}\,\mathrm{d}\theta-\mathrm{i}\frac{\mathrm{d}\left[\boldsymbol{C}_2\boldsymbol{G}_2^{(1)}\boldsymbol{A}_1^{\mathrm{T}}\right]}{\mathrm{d}\theta}\bigg|_{\theta=\theta_0+\pi/2}\right\} \tag{40}$$

$$\begin{aligned}
\frac{\partial \boldsymbol{S}\left(\boldsymbol{x}^{(2)};\boldsymbol{d}^{(1)}\right)}{\partial d_j}=-\frac{1}{2\pi r^3}\Bigg\{&\frac{2}{\pi}\int_0^{\pi}\frac{\boldsymbol{C}_2\boldsymbol{G}_2^{(1)}\left\langle g_j^{(1)}\right\rangle\boldsymbol{A}_1^{\mathrm{T}}}{\cos^3(\theta-\theta_0)}\,\mathrm{d}\theta+\mathrm{i}\Bigg[\frac{\mathrm{d}^2\left[\boldsymbol{C}_2\boldsymbol{G}_2^{(1)}\left\langle g_j^{(1)}\right\rangle\boldsymbol{A}_1^{\mathrm{T}}\right]}{\mathrm{d}^2\theta}\\
&+\left[\boldsymbol{C}_2\boldsymbol{G}_2^{(1)}\left\langle g_j^{(1)}\right\rangle\boldsymbol{A}_1^{\mathrm{T}}\right]\Bigg]\Bigg|_{\theta=\theta_0+\pi/2}\Bigg\}
\end{aligned} \tag{41}$$

When the field point is in material 1 and source point in material 2, we have

$$\begin{aligned}
&\boldsymbol{U}\left(\boldsymbol{x}^{(1)};\boldsymbol{d}^{(2)}\right)=\boldsymbol{U}\left(\boldsymbol{x}^{(1)};\boldsymbol{d}^{(1)}\right); \quad \frac{\partial \boldsymbol{U}\left(\boldsymbol{x}^{(1)};\boldsymbol{d}^{(2)}\right)}{\partial d_\alpha}=\frac{\partial \boldsymbol{U}\left(\boldsymbol{x}^{(1)};\boldsymbol{d}^{(1)}\right)}{\partial d_\alpha}\\
&\boldsymbol{T}\left(\boldsymbol{x}^{(1)};\boldsymbol{d}^{(2)}\right)=\boldsymbol{T}\left(\boldsymbol{x}^{(1)};\boldsymbol{d}^{(1)}\right); \quad \frac{\partial \boldsymbol{T}\left(\boldsymbol{x}^{(1)};\boldsymbol{d}^{(2)}\right)}{\partial d_\alpha}=\frac{\partial \boldsymbol{T}\left(\boldsymbol{x}^{(1)};\boldsymbol{d}^{(1)}\right)}{\partial d_\alpha}\\
&\boldsymbol{S}\left(\boldsymbol{x}^{(1)};\boldsymbol{d}^{(2)}\right)=\boldsymbol{S}\left(\boldsymbol{x}^{(1)};\boldsymbol{d}^{(1)}\right); \quad \frac{\partial \boldsymbol{S}\left(\boldsymbol{x}^{(1)};\boldsymbol{d}^{(2)}\right)}{\partial d_\alpha}=\frac{\partial \boldsymbol{S}\left(\boldsymbol{x}^{(1)};\boldsymbol{d}^{(1)}\right)}{\partial d_\alpha}
\end{aligned} \tag{42}$$

$$\frac{\partial \boldsymbol{U}\left(\boldsymbol{x}^{(1)};\boldsymbol{d}^{(2)}\right)}{\partial d_3}=\frac{-1}{2\pi r^2}\left\{\frac{1}{\pi}\int_0^{\pi}\frac{\overline{\boldsymbol{A}}_1\boldsymbol{G}_1^{(2)}\left\langle g_3^{(2)}\right\rangle\overline{\boldsymbol{A}}_2^{\mathrm{T}}}{\cos^2(\theta-\theta_0)}\,\mathrm{d}\theta-\mathrm{i}\frac{\mathrm{d}\left[\overline{\boldsymbol{A}}_1\boldsymbol{G}_1^{(2)}\left\langle g_3^{(2)}\right\rangle\overline{\boldsymbol{A}}_2^{\mathrm{T}}\right]}{\mathrm{d}\theta}\bigg|_{\theta=\theta_0+\pi/2}\right\} \tag{43}$$

$$\begin{aligned}
\frac{\partial \boldsymbol{T}\left(\boldsymbol{x}^{(1)};\boldsymbol{d}^{(2)}\right)}{\partial d_3}=\frac{1}{2\pi r^3}\Bigg\{&\frac{2}{\pi}\int_0^{\pi}\frac{\overline{\boldsymbol{B}}_1\boldsymbol{G}_1^{(2)}\left\langle g_3^{(2)}\right\rangle\overline{\boldsymbol{A}}_2^{\mathrm{T}}}{\cos^3(\theta-\theta_0)}\,\mathrm{d}\theta\\
&+\mathrm{i}\left[\frac{\mathrm{d}^2\left[\overline{\boldsymbol{B}}_1\boldsymbol{G}_1^{(2)}\left\langle g_3^{(2)}\right\rangle\overline{\boldsymbol{A}}_2^{\mathrm{T}}\right]}{\mathrm{d}^2\theta}+\left[\overline{\boldsymbol{B}}_1\boldsymbol{G}_1^{(2)}\left\langle g_3^{(2)}\right\rangle\overline{\boldsymbol{A}}_2^{\mathrm{T}}\right]\right]\Bigg|_{\theta=\theta_0+\pi/2}\Bigg\}
\end{aligned} \tag{44}$$

[4] If $\boldsymbol{x}=\boldsymbol{d}$, i.e., the field and source points coincide with each other, the traction vector and its derivative then experience a jump across the interface, characterized by the delta function $\delta(\boldsymbol{x}-\boldsymbol{d})$ and its derivative. This feature is similar to that of the corresponding Green's traction and its derivative in a homogeneous and anisotropic infinite space.

$$\frac{\partial \boldsymbol{S}\left(\boldsymbol{x}^{(1)};\boldsymbol{d}^{(2)}\right)}{\partial d_3}=\frac{1}{2\pi r^3}\left\{\frac{2}{\pi}\int_0^{\pi}\frac{\overline{\boldsymbol{C}}_1\boldsymbol{G}_1^{(2)}\left\langle g_3^{(2)}\right\rangle\overline{\boldsymbol{A}}_2^{\mathrm{T}}}{\cos^3(\theta-\theta_0)}\,\mathrm{d}\theta+\mathrm{i}\left[\frac{\mathrm{d}^2\left[\overline{\boldsymbol{C}}_1\boldsymbol{G}_1^{(2)}\left\langle g_3^{(2)}\right\rangle\overline{\boldsymbol{A}}_2^{\mathrm{T}}\right]}{\mathrm{d}^2\theta}+\left[\overline{\boldsymbol{C}}_1\boldsymbol{G}_1^{(2)}\left\langle g_3^{(2)}\right\rangle\overline{\boldsymbol{A}}_2^{\mathrm{T}}\right]\right]\Bigg|_{\theta=\theta_0+\pi/2}\right\} \tag{45}$$

Finally, when the field point is in material 2 and source point in material 2, these interfacial Green's functions are:

$$\begin{aligned}
&\boldsymbol{U}\left(\boldsymbol{x}^{(2)};\boldsymbol{d}^{(2)}\right)=\boldsymbol{U}\left(\boldsymbol{x}^{(1)};\boldsymbol{d}^{(2)}\right);\quad \frac{\partial \boldsymbol{U}\left(\boldsymbol{x}^{(2)};\boldsymbol{d}^{(2)}\right)}{\partial d_j}=\frac{\partial \boldsymbol{U}\left(\boldsymbol{x}^{(1)};\boldsymbol{d}^{(2)}\right)}{\partial d_j}\\
&\boldsymbol{T}\left(\boldsymbol{x}^{(2)};\boldsymbol{d}^{(2)}\right)=\boldsymbol{T}\left(\boldsymbol{x}^{(1)};\boldsymbol{d}^{(2)}\right);\quad \frac{\partial \boldsymbol{T}\left(\boldsymbol{x}^{(2)};\boldsymbol{d}^{(2)}\right)}{\partial d_j}=\frac{\partial \boldsymbol{T}\left(\boldsymbol{x}^{(1)};\boldsymbol{d}^{(2)}\right)}{\partial d_j}\\
&\boldsymbol{S}\left(\boldsymbol{x}^{(2)};\boldsymbol{d}^{(2)}\right)=\boldsymbol{S}\left(\boldsymbol{x}^{(2)};\boldsymbol{d}^{(1)}\right);\quad \frac{\partial \boldsymbol{S}\left(\boldsymbol{x}^{(2)};\boldsymbol{d}^{(2)}\right)}{\partial d_\alpha}=\frac{\partial \boldsymbol{S}\left(\boldsymbol{x}^{(2)};\boldsymbol{d}^{(1)}\right)}{\partial d_\alpha}
\end{aligned} \tag{46}$$

$$\frac{\partial \boldsymbol{S}\left(\boldsymbol{x}^{(2)};\boldsymbol{d}^{(2)}\right)}{\partial d_3}=\frac{\partial \boldsymbol{S}^{\infty}\left(\boldsymbol{x}^{(2)};\boldsymbol{d}^{(2)}\right)}{\partial d_3}-\frac{1}{2\pi r^3}\left\{\frac{2}{\pi}\int_0^{\pi}\frac{\boldsymbol{C}_2\boldsymbol{G}_2^{(2)}\left\langle g_3^{(2)}\right\rangle\overline{\boldsymbol{A}}_2^{\mathrm{T}}}{\cos^3(\theta-\theta_0)}\,\mathrm{d}\theta+\mathrm{i}\left[\frac{\mathrm{d}^2\left[\boldsymbol{C}_2\boldsymbol{G}_2^{(2)}\left\langle g_3^{(2)}\right\rangle\overline{\boldsymbol{A}}_2^{\mathrm{T}}\right]}{\mathrm{d}^2\theta}+\left[\boldsymbol{C}_2\boldsymbol{G}_2^{(2)}\left\langle g_3^{(2)}\right\rangle\overline{\boldsymbol{A}}_2^{\mathrm{T}}\right]\right]\Bigg|_{\theta=\theta_0+\pi/2}\right\} \tag{47}$$

Eqs. (33)–(47) are the *complete* interfacial Green's functions in anisotropic bimaterials, including the displacements, stresses, and their derivatives with respect to the source coordinates. These Green's functions are expressed in terms of finite-part integrals over $[0,\pi]$ with different orders of singularities, and possess the following important features:

1. Similar to the Green's functions in an anisotropic infinite space, the interfacial displacements, stresses and derivatives of displacements, and derivatives of stresses are inversely proportional, respectively, to r, r^2 and r^3 where r is the distance between the field and source points on the interfacial plane ($z=d=0$).
2. For the interfacial Green's functions that are inversely proportional to r, r^2 and r^3 their corresponding finite-part integral have singular orders of one ($1/\cos\theta$), two ($1/\cos^2\theta$), and three ($1/\cos^3\theta$), respectively.
3. Similar to the Green's functions in an anisotropic infinite space where the Green's functions in the whole space are completely determined by their values on a unit sphere (with field point on the unit sphere and source point at the center of the sphere), the interfacial Green's functions are completely determined by their values on the unit circles on the corresponding interfacial plane $z=0\pm$ and $d=0\pm$ (with field point on the unit circle and source point at the center of the circle).

4. Unlike the Green's displacement tensor in an anisotropic infinite space, which is symmetric, the interfacial Green's displacement tensor is not symmetric.

4. Numerical scheme on the calculation of finite-part integrals

Having derived the interfacial Green's functions and discussed their associated features, we now investigate how to carry out the 1D finite-part integration. Here, we present an adaptive integral scheme developed recently by the authors, with which the interfacial Green's functions can be evaluated accurately and efficiently.

Observation of the interfacial Green's functions reveals that each of them can be expressed as a sum of a finite-part integral and a constant term evaluated at $\theta = \theta_0 + \pi/2$. Therefore, to calculate the interfacial Green's functions, we only need to apply a suitable integral scheme for the evaluation of the finite-part integral. Furthermore, it is observed that there are, in general, three types (corresponding to the order $n = 1, 2, 3$) of the finite-part integrals, represented as

$$\boldsymbol{F}_n(\theta_0) = \int_0^{\pi} \frac{\boldsymbol{h}_n(\theta)}{\cos^n(\theta - \theta_0)}\,\mathrm{d}\theta; \quad n = 1, 2, 3 \tag{48}$$

Introducing a new variable $\phi = \theta - \theta_0 - \pi/2$ and utilizing the properties of the involved integrands, we can change (48) into

$$\boldsymbol{F}_n(\theta_0) = (-1)^n \int_{-\pi/2}^{\pi/2} \frac{\boldsymbol{h}_n(\varphi + \theta_0 + \pi/2)}{\sin^n \varphi}\,\mathrm{d}\varphi; \quad n = 1, 2, 3 \tag{49}$$

It is noted that, similar finite-part integrals (for $n = 1$ and 2) were used by Martin [27] when solving a flat crack problem in a 3D isotropic elastic solid. Using the singularity-subtraction method [23–25], these finite-part integrals can be regulated and expressed in the following integrable forms.

$$\begin{aligned}
\boldsymbol{F}_1(\theta_0) &= -\int_{-\pi/2}^{\pi/2} \frac{\boldsymbol{h}_1(\varphi + \theta_0 + \pi/2) - \boldsymbol{h}_1(\theta_0 + \pi/2)}{\sin\varphi}\,\mathrm{d}\varphi \\
\boldsymbol{F}_2(\theta_0) &= \int_{-\pi/2}^{\pi/2} \left\{ \frac{\boldsymbol{h}_2(\varphi + \theta_0 + \pi/2) - \boldsymbol{h}_2(\theta_0 + \pi/2)}{\sin^2\varphi} - \frac{\boldsymbol{h}_2'(\theta_0 + \pi/2)}{\sin\varphi} \right\} \mathrm{d}\varphi \\
\boldsymbol{F}_3(\theta_0) &= -\int_{-\pi/2}^{\pi/2} \left\{ \frac{\boldsymbol{h}_3(\varphi + \theta_0 + \pi/2) - \boldsymbol{h}_3(\theta_0 + \pi/2)}{\sin^3\varphi} - \frac{\boldsymbol{h}_3'(\theta_0 + \pi/2)}{\sin^2\varphi} - \frac{\boldsymbol{h}_3''(\theta_0 + \pi/2)}{2\sin\varphi} \right\} \mathrm{d}\varphi
\end{aligned} \tag{50a, b, c}$$

Where the primes $'$ and $''$ denote the first and second derivatives of the associated functions. Also, in deriving (50a–c), the following finite-part integral results, which can be verified numerically using the definition for the finite-part integral [23–25], have been used:

$$\int_{-\pi/2}^{\pi/2} \frac{1}{\sin^n \varphi}\,\mathrm{d}\varphi = 0; \quad n = 1, 2, 3 \tag{51}$$

Since the integrals in (50a–c) are all regular, they can be easily calculated by any numerical quadrature. Here, the adaptive integral scheme with quadratic interpolation in each subinterval [28] is used to calculate these integrals accurately.

5. Numerical examples

Each of the interfacial Green's functions derived in this paper has been tested for different material pairs. These include the transversely isotropic and isotropic bimaterials, anisotropic infinite space (materials 1 and 2 have the same elastic constants), and anisotropic half-space (one of the material domains has zero elastic constants). In the following, one of the material pairs is selected for illustration.

Material 1 ($z > 0$ domain) is orthotropic with $E_1 = 206.84$ GPa, $E_2 = E_3 = 20.684$ GPa, $G_{13} = G_{23} = G_{12} = 6.895$ GPa, and $\nu_{13} = \nu_{23} = \nu_{12} = 0.336$ [29]. When converted to the stiffness matrix C_{ij} and normalized with respect to E_1 we obtained the stiffness matrix C_{ij} given in Table 1. A fully popular stiffness matrix is used for material 2 ($z < 0$ domain) and its elements are listed in Table 2. This stiffness matrix was obtained by rotating the symmetric plane of a transversely isotropic material with respect to its material coordinates [21].

With the material properties given in Tables 1 and 2 and the adaptive numerical integration scheme, we have calculated the interfacial Green's functions (33)–(47) for the field points on the unit circle and source point at the center of the circle (i.e., $r = 1$). We mention that no specific unit is given for the interfacial Green's functions presented below.

Figs. 2 and 3 show the variation of the interfacial displacements, tractions, and their derivatives on the unit circle. The derivative is taken with respect to the source coordinate in the x-direction (i.e., with respect to d_1). In the legend of these figures, the first and second subscripts are the component of displacement or traction, and the direction of the point force, respectively. The definition of the traction components is given by (6a), that is

Table 1
Stiffness matrix C_{ij} in material 1 ($z > 0$ domain)

1.0352019	0.0523837	0.0523837	0.0	0.0	0.0
–	0.1153771	0.0405268	0.0	0.0	0.0
–	–	0.1153771	0.0	0.0	0.0
–	–	–	0.0333333	0.0	0.0
–	–	–	–	0.0333333	0.0
–	–	–	–	–	0.0333333

Table 2
Stiffness matrix C_{ij} in material 2 ($z < 0$ domain)

1.45	0.99	0.96	−0.02	−0.31177	−0.15588
–	1.85	0.96	−0.22	−0.10392	−0.19052
–	–	1.28	−0.16	−0.27713	0.0
–	–	–	0.32	0.0	−0.10392
–	–	–	–	0.32	−0.02
–	–	–	–	–	0.35

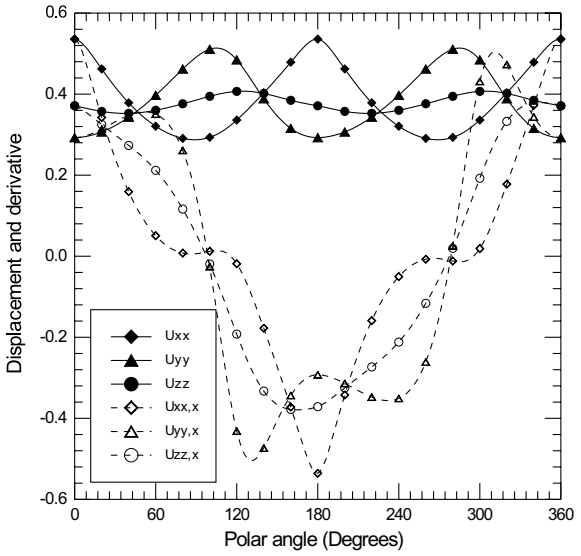

Fig. 2. Interfacial displacements and their derivatives with respect to the source coordinate in the x-direction (i.e., with respect to d_1).

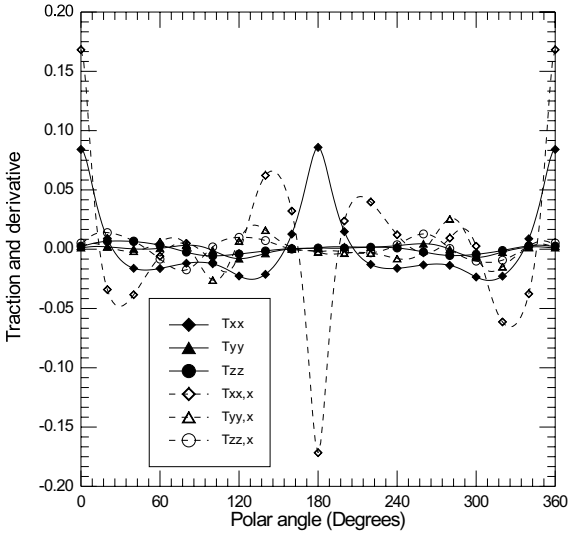

Fig. 3. Interfacial tractions and their derivatives with respect to the source coordinate in the x-direction (i.e., with respect to d_1).

$$(T_x, T_y, T_z) \equiv (\sigma_{13}, \sigma_{23}, \sigma_{33}) \tag{52}$$

We remark that these interfacial Green's functions (displacements and tractions) and their derivatives with respect to the horizontal source coordinate are the same on both sides of the interface (for $z = 0\pm$ and $d = 0\pm$). In other words, they are continuous across the interface.

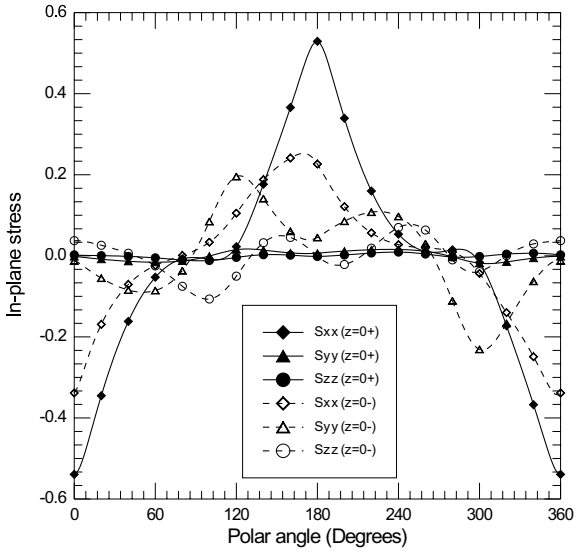

Fig. 4. Interfacial in-plane stresses above ($z = 0+$) and below ($z = 0-$) the interface.

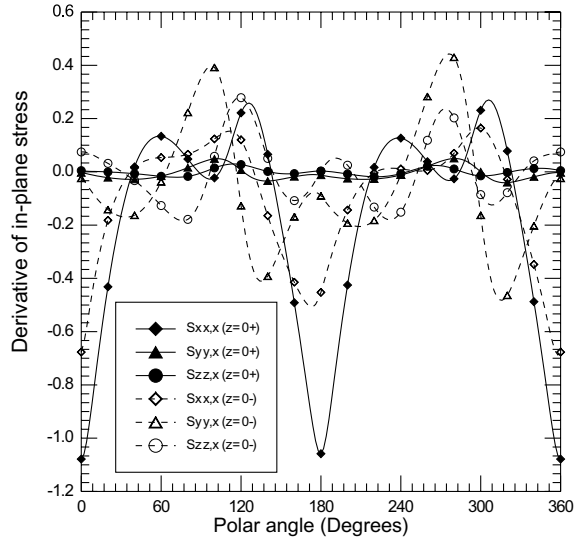

Fig. 5. Derivatives of the interfacial in-plane stresses above ($z = 0+$) and below ($z = 0-$) the interface, with respect to the source coordinate in the x-direction (i.e., with respect to d_1).

Depicted in Figs. 4 and 5 are the variation of the in-plane stresses and their derivatives on the unit circle (for $d = 0\pm$). Again, the derivative is taken with respect to the source coordinate in the x-direction (i.e., with respect to d_1). Similar to Fig. 3, the second subscript in the legend denotes the direction of the point force, and the first subscript is for the component of the in-plane stress vector defined by (6b), that is

$$(S_x, S_y, S_z) \equiv (\sigma_{11}, \sigma_{12}, \sigma_{22}) \tag{53}$$

It is obvious that the in-plane stresses just above ($z = 0+$) and below ($z = 0-$) the interface are completely different and therefore the vertical component (z) of the field point needs to be clearly distinguished when discussing the interfacial in-plane stresses.

Finally, Figs. 6 and 7 show the variation of the derivatives of the in-plane stresses on the unit circle. The derivative is now taken with respect to the source coordinate in the z-direction (i.e.,

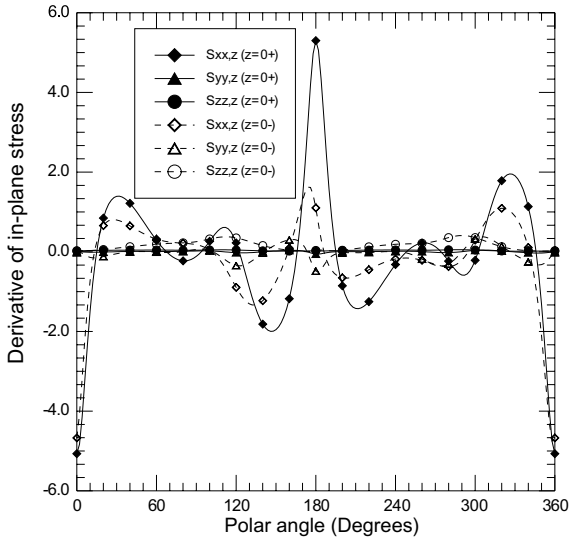

Fig. 6. Derivatives of the interfacial in-plane stresses with respect to the source coordinate in the z-direction above the interface ($d = 0+$) with $z = 0+$ for results above the interface, and $z = 0-$ for these below the interface.

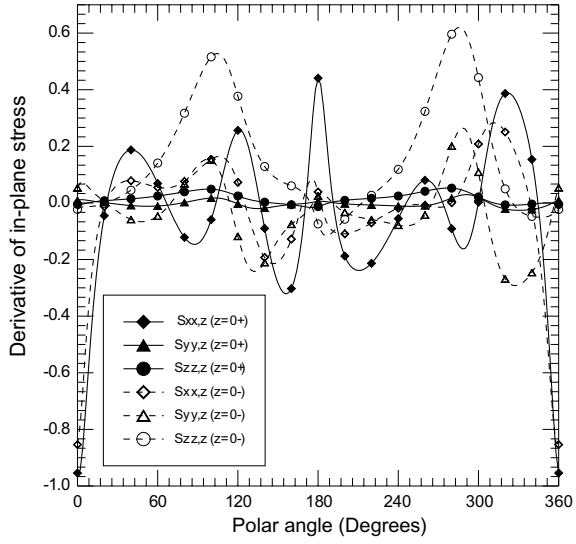

Fig. 7. Derivatives of the interfacial in-plane stresses with respect to the source coordinate in the z-direction below the interface ($d = 0-$) with $z = 0+$ for results above the interface, and $z = 0-$ for these below the interface.

with respect to $d_3 \equiv d$). While in Fig. 6, the derivatives are carried out for the source point just above the interface ($d = 0+$), in Fig. 7, they are for the source point just below the interface ($d = 0-$). These two figures illustrate the dependence of the derivatives of the interfacial Green's functions in general, and of the in-plane stresses in particular, upon the third source coordinate d as related to the interface.

6. Conclusions

In this paper, we have derived, *for the first time*, the *complete* three-dimensional interfacial Green's functions in anisotropic bimaterials, which include the displacements, stresses, and their derivatives with respect to the source coordinates. They are expressed in terms of 1D finite-part integrals over $[0, \pi]$ with the regular part of their integrands consisting of the extended Stroh eigenvalues and eigenvectors. Four important features associated with these interfacial Green's functions have been observed:

1. The interfacial displacements, stresses and derivatives of displacements, and derivatives of stresses are inversely proportional, respectively, to r, r^2 and r^3 where r is the distance between the field and source points on the interfacial plane ($z = d = 0$).
2. For the interfacial Green's functions that are inversely proportional to r, r^2 and r^3 their corresponding finite-part integrals have singular orders of one ($1/\cos\theta$), two ($1/\cos^2\theta$), and three ($1/\cos^3\theta$), respectively.
3. The interfacial Green's functions are completely determined by their values on the unit circles on the corresponding interfacial planes $z = 0\pm$ and $d = 0\pm$ (with the field point on the unit circle and the source point at the center of the circle).
4. The interfacial Green's displacement tensor is not symmetric.

We further point out that although the third-order singularity ($1/\cos^3\theta$) was previously discussed mathematically, no physical quantity has ever been associated to it. In this paper, we have shown that in the derivation of the derivative of the interfacial Green's stresses in anisotropic bimaterials, the third-order singularity ($1/\cos^3\theta$) is involved.

To evaluate the involved 1D finite-part integrals, an efficient and accurate numerical method has also been proposed. Numerical examples are presented, illustrating the variation of some of the interfacial Green's functions along the unit circles on the corresponding interface planes. These examples clearly demonstrate the discontinuity features of some of the Green's functions across the interface.

Acknowledgements

This project is supported in part by the AFOSR under grant no. F33615-97-C-5089. Dr. Richard Hall is the project manager.

Appendix A. Derivative of the interfacial traction with respect to the source coordinates

First, we take the derivative of the bimaterial traction (when both the source and field points are in material 1, i.e., $z > 0$ and $d > 0$) and then take the limit to find

$$\left.\frac{\partial \boldsymbol{t}_1(\boldsymbol{x};\boldsymbol{d})}{\partial d_j}\right|_{(z,d)=(0+,0+)} = \left.\frac{\partial \boldsymbol{t}_1^{\infty}(\boldsymbol{x};\boldsymbol{d})}{\partial d_j}\right|_{(z,d)=(0+,0+)} - \frac{\mathrm{i}}{4\pi^2}\left[\int_0^{\pi}\mathrm{d}\theta\int_0^{\infty}\overline{\boldsymbol{B}_1}\boldsymbol{G}_1^{(1)}\langle g_j^{(1)}\rangle\boldsymbol{A}_1^{\mathrm{T}}\eta^2\mathrm{e}^{-\mathrm{i}\eta[(x_1-d_1)\cos\theta+(x_2-d_2)\sin\theta]}\,\mathrm{d}\eta\right]\boldsymbol{f} \tag{A.1}$$

where $\langle g_j^{(1)}\rangle$ are the three diagonal matrices defined by Eq. (25), and the first term on the right-hand side has been replaced by the infinite-space Green's function [21]. Since an explicit expression for the infinite-space Green's function is available [21], we only need to study the second term on the right-hand side of (A.1). Therefore, the infinite-space Green's function will be omitted in the following discussion for brevity.

Now, we make use of the polar coordinate transform (32) to arrive at the following expression

$$\left.\frac{\partial \boldsymbol{t}_1(\boldsymbol{x};\boldsymbol{d})}{\partial d_j}\right|_{(z,d)=(0+,0+)} = -\frac{\mathrm{i}}{4\pi^2}\left[\int_0^{\pi}\mathrm{d}\theta\overline{\boldsymbol{B}}_1\boldsymbol{G}_1^{(1)}\langle g_j^{(1)}\rangle\boldsymbol{A}_1^{\mathrm{T}}\int_0^{\infty}\eta^2\mathrm{e}^{-\mathrm{i}\eta r\cos(\theta-\theta_0)}\,\mathrm{d}\eta\right]\boldsymbol{f} \tag{A.2}$$

where we have also used the fact that all the matrices are independent of η. To carry out the integral with respect to η, one needs to use (31), which in the present case, is

$$\int_0^{\infty}\eta^2\mathrm{e}^{-\mathrm{i}\eta r\cos(\theta-\theta_0)}\,\mathrm{d}\eta = \frac{2\mathrm{i}}{r^3\cos^3(\theta-\theta_0)} - \pi\delta''[r\cos(\theta-\theta_0)] \tag{A.3}$$

Therefore, Eq. (A.2) becomes

$$\left.\frac{\partial \boldsymbol{t}_1(\boldsymbol{x};\boldsymbol{d})}{\partial d_j}\right|_{(z,d)=(0+,0+)} = -\frac{\mathrm{i}}{4\pi^2}\left[\int_0^{\pi}\overline{\boldsymbol{B}}_1\boldsymbol{G}_1^{(1)}\langle g_j^{(1)}\rangle\boldsymbol{A}_1^{\mathrm{T}}\,\mathrm{d}\theta\left\{\frac{2\mathrm{i}}{r^3\cos^3(\theta-\theta_0)} - \pi\delta''[r\cos(\theta-\theta_0)]\right\}\right]\boldsymbol{f} \tag{A.4}$$

In order to finally find the derivative of the interfacial traction with respect to the source coordinates, one needs to find the contribution from the delta function. It can be shown that for a function $h(\theta) \in C^2$ the following relation holds,

$$\int_0^{\pi}h(\theta)\delta''[r\cos(\theta-\theta_0)]\,\mathrm{d}\theta = \frac{1}{r^3}\left[h''(\theta)+h(\theta)\right]\Big|_{\theta=\theta_0+\pi/2} \tag{A.5}$$

Making use of this relation, we finally find the derivative of the interfacial traction with respect to the source coordinates, as given by Eq. (36).

References

[1] E. Pan, A BEM analysis of fracture mechanics in 2D anisotropic piezoelectric solids, Eng. Anal. Bound. Elem. 23 (1999) 67–76.

[2] J.R. Berger, V.K. Tewary, Green's functions for boundary element analysis of anisotropic bimaterials, Eng. Anal. Bound. Elem. 25 (2001) 279–288.
[3] N.J. Pagano, Stress fields in composite laminates, Int. J. Solids Struct. 11 (1978) 385–400.
[4] N.J. Pagano, Free edge stress fields in composite laminates, Int. J. Solids Struct. 14 (1978) 401–406.
[5] D.M. Barnett, J. Lothe, Line force loadings on anisotropic half-spaces and wedges, Physica Norvegica 8 (1975) 13–22.
[6] J.J. Vlassak, W.D. Nix, Measuring the elastic properties of anisotropic materials by means of indentation experiments, J. Mech. Phys. Solids 42 (1994) 1223–1245.
[7] E. Pan, Static Green's functions in multilayered half spaces, Appl. Math. Modeling 21 (1997) 509–521.
[8] J.J. Liao, C.D. Wang, Elastic solutions for a transversely isotropic half-space subjected to a point load, Int. J. Numer. Anal. Meth. Geomech. 22 (1998) 425–447.
[9] C.D. Wang, J.J. Liao, Elastic solutions for a transversely isotropic half-space subjected to buried asymmetric-loads, Int. J. Numer. Anal. Meth. Geomech. 23 (1999) 115–139.
[10] J.C. Lee, L.M. Keer, Study of a three-dimensional crack terminating at an interface, ASME, J. Appl. Mech. 53 (1986) 311–316.
[11] W. Lin, C.H. Kuo, L.M. Keer, Analysis of a transversely isotropic half space under normal and tangential loadings, ASME J. Tribol. 113 (1991) 335–338.
[12] H. Noguchi, R.A. Smith, An analysis of a semi-infinite solid with three-dimensional cracks, Eng. Fract. Mech. 52 (1995) 1–14.
[13] M.C. Chen, N.A. Noda, R.J. Tang, Application of finite-part integrals to planar interfacial fracture problems in three-dimensional bimaterials, ASME J. Appl. Mech. 66 (1999) 885–980.
[14] E. Pan, B. Yang, Elastostatic fields in an anisotropic substrate due to a buried quantum dot, J. Appl. Phys. 90 (2001) 6190–6196.
[15] H. Lee et al., Controlled ordering and positioning of InAs self-assembled quantum dots, J. Vac. Sci. Technol. B 18 (2000) 2193–2196.
[16] J.S. Kim et al., Energy level control for self-assembled InAs quantum dots utilizing a thin AlAs layer, Appl. Phys. Lett. 78 (2001) 3247–3249.
[17] T.C.T. Ting, Anisotropic Elasticity, Oxford University Press, Oxford, 1996.
[18] E. Pan, B. Amadei, Boundary element analysis of fracture mechanics in anisotropic bimaterials, Eng. Anal. Bound. Elem. 23 (1999) 683–691.
[19] E. Pan, F.G. Yuan, Three-dimensional Green's functions in anisotropic bimaterials, Int. J. Solids Struct. 37 (2000) 5329–5351.
[20] T.C.T. Ting, V.G. Lee, The three-dimensional elastostatic Green's function for general anisotropic linear elastic solids, Quart. J. Mech. Appl. Math. 50 (1997) 407–426.
[21] F. Tonon, E. Pan, B. Amadei, Green's functions and boundary element method formulation for 3d anisotropic media, Comput. Struct. 79 (2001) 469–482.
[22] E. Pan, Three-dimensional Green's functions in anisotropic magneto-electro-elastic bimaterials, J. Appl. Math. Phys. (ZAMP) 53 (2002) 815–838.
[23] D.F. Paget, The numerical evaluation of Hadamard finite-part integrals, Numer. Math. 36 (1981) 447–453.
[24] G. Monegato, Numerical evaluation of hypersingular integrals, J. Comput. Appl. Math. 50 (1994) 9–31.
[25] N. Mastronardi, D. Occorsio, Some numerical algorithms to evaluate Hadamard finite-part integrals, J. Comput. Appl. Math. 70 (1996) 75–93.
[26] K.C. Wu, Generalization of the Stroh formalism to 3-dimensional anisotropic elasticity, J. Elasticity 51 (1998) 213–225.
[27] P.A. Martin, Mapping flat cracks onto penny-shaped cracks: shear loadings, J. Mech. Phys. Solids 43 (1995) 275–294.
[28] W.H. Press et al., Numerical Recipes: The Art of Scientific Computing, 1989.
[29] E. Pan et al., Stress analyses around holes in composite laminates using boundary element method, Eng. Anal. Bound. Elem. 25 (2001) 31–40.